A High Resolution Fourier-Transform UV-Visible Spectrometer for the Measurement of Atmospheric Column Abundances

R. P. Cageao, J.-F. Blavier, J. P. McGuire, Y. Jiang, V. Nemtchinov, and S. P. Sander,

Abstract

A compact, high resolution Fourier-transform spectrometer for atmospheric near ultraviolet spectroscopy has been installed at the Jet Propulsion Laboratory's Table Mountain Facility (34.4 N, 117.7 W, elevation 2290m). This instrument is designed with an unapodized resolving power near 500,000 at 300 nm to provide high resolution spectra from 290 to 675 nm for the quantification of column abundances of trace species such as OH, NO_3, O_3, NO_2, and BrO. The measurement techniques used include spectral analysis of terrestrial absorptions of direct solar and lunar radiation and multiply scattered solar radiation observed in the zenith sky. The instrument, accompanying systems designs, and preliminary results are described herein.

Key words: Atmospheric spectroscopy, Fourier-transform interferometer, hydroxyl column, UV-visible

1. Introduction

Validation of models of kinetics, photochemistry, and transport requires a large measurement database. Transient species such as OH, NO_3, BrO, and ClO are particularly important because these reactive free-radical species play key roles in the processes that catalytically destroy ozone. In the visible and near ultraviolet, some of these species have large electronic transition cross-sections, simplifying detection. Discrimination of the absorption features of these species in the highly structured direct or backscattered solar spectrum requires high spectral resolution to separate vibrational and rotational band structure.

In the upper stratosphere, above 50km, catalytic ozone destruction cycles are dominated by the HOx family (OH, HO_2, and H). OH is produced in the stratosphere and mesosphere predominantly from water photolysis and reaction with $O(^1D)$, a byproduct of ozone photodissociation. OH participates in the destruction of odd oxygen, including ozone, and the recombination of CO with O forming CO_2. In the middle and lower stratosphere, the HOx family is involved in odd nitrogen, odd chlorine, and odd oxygen chemistry. OH participates directly and indirectly in ozone catalytic destruction and moderates the effects of odd chlorine and odd nitrogen by aiding in the sequestration of these species in their reservoir molecular forms. OH is expected to vary temporally, seasonally, and latitudinally due to the distribution of its precursors, H_2O and CH_4 and penetration of short wavelength radiation which produces photolytic OH precursors.

Measurements of OH abundance and its variation seasonally and diurnally are both scientifically important to the understanding of upper atmospheric chemistry and technically difficult. Several techniques have been applied to OH measurements in the lower stratosphere using *in situ* laser-induced fluorescence[1-2] and far-infrared spectroscopy,[3-6] and in the mesosphere and upper stratosphere using near ultraviolet spectroscopy.[7-9] Only a few of the ground-based installations using a poly-etalon Fabry-Perot,[10-12] grating instrument,[13-14] or interferometer[15] have an extended data record of the vertical column of OH that allows the analysis of temporal OH variations and their relation to the upper atmospheric chemistry.

A Fourier-transform spectrometer instrument has the decided advantages of large throughput, high spectral resolution, multiple absorption line detection, parasitic light insensitivity, and wide wavelength coverage over several of the techniques listed above. For several years infrared Fourier transform spectrometers have been used effectively in laboratory and atmospheric spectroscopy.[5,16-17] In the visible and near ultraviolet, however, their use has been limited due to the complexities of instrument design and coating manufacture necessary to preserve the transmitted wavefront and interferometric contrast through the instrument. Because of the advantages inherent in the Fourier transform spectrometer design, a Fourier Transform Ultraviolet Spectrometer (FTUVS) was developed for use in the near ultraviolet and was used to quantify the vertical column abundance of OH. The design of the instrument, and

experience using it to measure the vertical and slant column of OH in a direct solar absorption mode at a field installation is discussed below.

2. Instrument Description

A. System Description

The FTUVS system is located at the Table Mountain Facility (34.4 N, 117.7 W, elevation 2290 m). The instrument is comprised of the three basic subsystems shown in Figure 1: 1) a heliostat for tracking the sun or moon to provide a background spectrum for the detection of terrestrial absorption features, 2) a matched etendue telescope which collects and reduces the beam size of the source for input to the interferometer and provides a feedback image for closed loop tracking, and 3) an interferometer which records spectra of the selected source (sun, moon, or zenith sky). In addition, a data acquisition and instrument control system allows co-adding of multiple spectral scans to improve the photon limited signal to noise ratio.

The heliostat, constructed by DFM Engineering of Longmount, CO, is located on the second floor of the building within the dome structure and is exposed to the outside ambient conditions. The heliostat primary and secondary mirrors, 50.8 and 32 cm Zerodur substrates, respectively, both aluminum coated with SiO_2 and MgF_2 overcoats, were sized to provide an unvignetted 0.5 degree field of view and a 20cm diameter

beam to the telescope aperture stop. The equatorially mounted heliostat primary mirror is driven in Right Ascension and Declination to track any celestial object at a selected rate with an accuracy of 1.8 arcsec/min.

The light beam reflected from the heliostat and then downward from second floor dome area passes through a 25cm UV grade fused silica window with 15arcmin wedge before reaching the first floor temperature controlled instrument room. In the instrument room the beam passes through the telescope aperture stop before reaching the afocal Gregorian telescope primary. The telescope consists of confocal parabolic mirrors mounted on an Invar rod for thermal stability. The telescope off-axis parabola design is free from spherical aberration, coma, and astigmatism. The design also minimizes reflection losses by using only two reflecting surfaces to compress the beam. The off-axis parabola telescope optics are aluminum coated, SiO_2 and MgF_2 overcoated, with $\lambda/8$ wavefront accuracy and have standard, off-the-shelf focal lengths. The telecope primary is an f/3.2, 20 cm diameter off-axis segment of a parabolic mirror which focuses the light beam onto a reflective field stop. The field stop aperture allows part of the focused image to pass through to one of two telescope secondary mirrors where it is recollimated by an f/3.2, 6.4 cm diameter parabolic mirror for delivery to the FTUVS interferometer. The rest of the image is reflected off the oxygen free cooper, aluminum coated, water-cooled field stop toward a 3.3 cm diameter f=30.5 cm parabolic secondary. This mirror collimates the light and delivers it through neutral density filters to a Nikkon f=135 mm lens, and a Vivitar 2x converter focused onto a Cohu Model 7420 CCD image plane. The image is displayed on a standard 12 inch television monitor

Epix frame grabbing board. This image is then displayed on a tracking computer monitor and analyzed using a Visual Basic program written at JPL. The image position in the CCD frame is used to provide closed loop tracking correction signals to the heliostat motor driver. The complete closed loop system can track a celestial object with an accuracy of 10 arcsec/min up to zenith angles of 85 degrees.

B. Interferometer Description

Two turning mirrors direct the collimated light beam from the telescope through a 7.5cm diameter bandpass limiting interference filter and then toward the FTUVS interferometer (shown schematically in Figure 2). The FTUVS, turning mirrors, interference filter, and telescope are all mounted on the same pneumatically isolated optical table. The FTUVS was designed and built at the Jet Propulsion Laboratory. It is a flex-pivot supported, voice coil actuated, active-aligned plane mirror interferometer with an entendue of 2×10^{-4} cm^2-ster.[18] Plane mirrors were chosen to minimize the number of reflections and reduce wavefront distortion. The interferometer moving mirror mechanism is a parallelogram consisting of four tubes constructed from 152μm thick rolled Invar for thermal and mechanical stability, connected by eight Bendix flex pivots. The lower, horizontal side of the parallelogram supports a mirror. This arm of the parallelogram is driven by a voice coil actuator in along an essentially frictionless "porch swing" path moving the mirror horizontally 5cm. The mirror is moved at a constant velocity by a Hewlett-Packard (HP) Model 5507A Laser Positioning System (LPS) servo-axis driver. This system uses a 2.1Mhz Zeeman split, linearly polarized,

two-frequency He-Ne laser. The polarized beams are split one each into the two interferometer arms by a small polarizing spot coating on the beamsplitter front surface. The Doppler shifted frequency of the beam from the moving mirror arm is compared to the laser reference frequency for measurement and control of scan mirror velocity. The He-Ne beam is also used to produce an interferogram sampling trigger signal by mixing the 2.1Mhz Zeeman split laser reference frequency with the Doppler shifted moving mirror arm laser frequency to produce a laser fringe marker.

The stability of this system to mirror tilt is better than 1μrad over 1cm of travel. To achieve the desired mirror tilt stability of 0.1μrad over 5 cm of mechanical travel (to maintain high fringe contrast at high spectral resolution), an active tilt compensation system was added using a servo-controlled, piezo-electric actuator driving the fixed mirror to match the moving mirror tilt.[19] The servo is activated by three miniature HP photodiodes sensing the phase of the 6mm diameter HP LPS He-Ne laser reference beam at three places in the beam. A phase comparator determines the phase mismatch and produces the voltage that is required to drive the three piezo stacks behind the fixed mirror and reduce the phase mismatch.

Optics for the interferometer, the beamsplitter, compensator, and mirror substrates were figured by IC Optical of Great Britain. Coatings on the interferometer mirrors are aluminum with an SiO_2 overcoat. The interferometer beamsplitter has a multi-layer dielectric coating, applied by Barr Associates, Inc. with 50 to 30% reflectivity 250 - 650nm at 45 degrees incidence angle. Barr also applied the beamsplitter He-Ne

polarizing spot. For observations of column OH, a narrow bandpass interference filter, 75mm in diameter, is placed near the entrance to the interferometer. Its bandpass is centered at 307.8 nm where the peak transmission is 45%. The full-width-half-maximum (FWHM) of this filter is 3.8nm and out of band rejection is greater than 10^{-7}. The filter is used to isolate the strongest OH rotational absorption lines in the (0,0) vibrational band, $X^2\Pi \rightarrow A^2\Sigma$ electronic transition. The FTUVS interferometer has been operated successfully with these components (excluding bandpass filter) from 290 to 675nm. Alternative coatings applied to a second beamsplitter, could extend the spectral detection range longward of 675nm to 1500nm.

C. Instrument Operation Modes

The principal observation mode is direct solar imaging and spectral analysis to detect the imbedded terrestrial absorption lines. Variations in the depth of the terrestrial absorption features are linked to the vertical column abundance. The extraction of terrestrial absorption features from the solar spectrum is simplified by observing opposing limbs of the sun. The induced Doppler shift due to the 27 day rotation period at the solar equator shifts the solar spectral features relative to stationary terrestrial absorption features (Figure 3). This characteristic can be used to separate the solar Fraunhofer features from the terrestrial absorption features. The equatorial Doppler shift between the east and west limbs of the sun is 0.38 cm^{-1}. By observing the solar West limb and shifting it in spectral frequency to match an East limb spectrum, the Fraunhofer features can be removed leaving terrestrial absorptions.

Other instrument operation modes have been employed successfully. These include: 1) full disk lunar observations at 15,106cm^{-1} (662nm) with a spectral resolution of 1.5cm^{-1}, ratioing moonrise in twilight to moonset in darkness for nighttime abundances of NO_3, 2) Rayleigh and multiply scattered near-UV sunlight observations of the zenith sky at high solar zenith angles and lower spectral resolution (5.7cm^{-1}) for the detection of O_3 and NO_2 and 3) high and low solar zenith angle ratioed direct solar imaged observations for the detection of NO_2.

D. Data System

An Advanced Photonics avalanche photodiode measures the UV analog signal passing through the interferometer. A transimpedance amplifier converts the detector output current into a voltage. A low-pass Bessel electronic filter insures that high frequencies in the output signal are not aliased into the observed spectral bandpass. The signal is converted into 16-bit digital words with an Analogic ADC5020 analog to digital converter. The sampling pulses used to trigger the conversion are derived from the zero crossings of the He-Ne laser fringes using a Phase-Locked Loop (PLL). This PLL also multiplies the laser fringe crossing frequency (typically 6 to 12 kHz) by a factor between 1 and 15 (usually 6 or 8). The Voltage Controlled Oscillator (VCO), a CD4046, of the PLL was selected for low jitter noise. The phase detector of the PLL, critical for best performance, is a symmetrical design, which was implemented using a fast Erasable Programmable Logic Device (Altera EP610I-10ns). The PLL filter is an

active design, with additional high frequency removal to minimize He-Ne laser frequency ghosts. The -3dB frequency of that filter is 125 Hz, a compromise between laser frequency rejection and the highest frequency in the spectrum of the scanner velocity errors. The digital data interface is based around a transputer link adapter, sending the data to a PC board (INMOS IMS-B008) carrying transputer modules manufactured by Transtech and INMOS. The transputer network also controls the PLL, the HP laser positioning system drive commands (via an HPIB bus), and a 4Gb data storage disk drive (SCSI bus). The disk drive records the full interferogram data stream, and the entire system can sustain data rates up to 10^5 samples per second at two bytes per sample.

E. Data Reduction

The transputer array performs post-acquisition manipulation of the instrument-acquired interferograms. A short section around zero path difference (typically 16k points) of the digitized interferogram is used to measure the phase of each interferogram.[20] With this phase information and the spectral domain selected by a digital filter, a time-domain operator is derived which is used to phase correct the nearly single-sided interferograms.[21] Each phase-corrected and filtered interferogram is then fast Fourier analyzed to produce individual spectra. These spectra are then summed and averaged in memory for the desired period of data acquisition. For the OH column observations, spectra are collected over a 15-minute period at each solar limb. On a separate PC platform these summed East and West limb solar spectra are interpolated on a finer

grid by convolving the spectrum with a sinc function of a width determined by the instrument scan parameters. The necessary spectral shift (approximately 0.28cm^{-1}) to be applied to the West limb data to match the solar Fraunhofer features of the East limb spectrum is determined by minimizing the residuals in a linear least squares matching of the two spectra. The East limb spectrum is then divided by the shifted West limb spectrum. The terrestrial OH absorption feature appears in the ratio as either a reduction in the ratio (terrestrial OH absorption in the East limb spectrum divided by the West limb solar background) or as an increase in the ratio (East limb background divided by OH absorption in the West limb spectrum). The residual baseline slope is then removed and the absorption signatures of 5 to 7 OH absorption lines are fitted to a synthetic instrument line shape convolved with an aperture broadened Doppler line shape for OH at 250K. This synthetic OH absorption line fit is adjusted to minimize the square deviation between the fit and measured spectrum on a grid of line strength versus synthetic feature spectral position (see Figure 4). The resulting measured line strength and the calculated absorption cross section of the line are then used to determine the slant column of OH. This is converted to vertical column abundance by dividing the slant column by the airmass (secant of the solar zenith angle). Observations are obtained for airmasses up to 5 (object zenith angles of 78 degrees).

3. Results

Figure 5 presents a single day of measured OH vertical column and its diurnal variation. Each point is derived from a 15 minute integration West limb followed by a 15 minute integration East limb. Vertical bars represent the 1σ statistical error in derived OH column from uncertainties in the match between synthetic fit and measured OH features. The derived OH column is obtained from the weighted average of two strongest OH absorption lines. Several hundred of these OH diurnal column data sets have been acquired starting in July 1997 for solar zenith angles of 10 to 78 degrees (airmasses 1.02 to 5.0). The signal to noise ratio for these 15 minute integration data sets is estimated to be 800:1 at the filter bandpass peak and 80:1 at the Fraunhofer minima where most of the telluric OH absorption features lie.

A total OH column measurement uncertainty can be derived by adding in quadrature uncertainties in laboratory measured line center cross section, the matching of the synthetic fit to the observed absorption features, the effect of residual spectral "features", detector photon counting statistics, and an object tracking system error budget. These uncertainties are outlined in Figure 6. The conservatively estimated measurement uncertainty is 20 to 22%.

4. Conclusions

We have demonstrated a compact, high resolution, actively aligned Fourier transform spectrometer for UV-visible atmospheric spectroscopy, have applied it to the measurement of OH column, and have begun analysis of similar data for NO_3, NO_2, and O_3 columns in the terrestrial atmosphere. The capabilities of this instrument will be exercised in an attempt to measure, ClO, BrO, IO, OClO columns as well as other atmospheric free radicals, exploiting the broad spectral coverage and high resolution of the instrument. The instrument is located at the JPL Table Mountain Facility site adjacent to a JPL tropospheric ozone/aerosol Lidar, a JPL stratospheric ozone/aerosol/temperature Lidar, a Naval Research Laboratory H_2O microwave radiometer, and often the JPL MkIV infrared interferometer. Coupling UV-visible and IR interferometry with lidar and microwave radiometry data to investigate the changes in, and the interactions of, HOx, NOx and ClOx families with ozone will be pursued using the unique TMF data base and atmospheric models developed at the California Institute of Technology.

Acknowledgments

The research described in this work was conducted at the Jet Propulsion Laboratory, California Institute of Technology. It was supported by grants from the NASA Upper Atmosphere Research Program, the Naval Research Laboratory, and by the Jet Propulsion Laboratory Director's Discretionary Fund. We would like to thank R. Beer, B. Farmer, R. Norton, R. Friedl, D. Peterson, and G. Toon of JPL and G. Wyntjes and J. Engel of Optra, Inc. for many valuable discussions. We also thank D. Miller, J. MacConnell, G. A. Al-Jumaily, D. Natzic, R. Chave, R. Marquedant, J. Voeltz, and B. Wilson for assistance in the instrument design and fabrication.

Author Affiliations:

R. P. Cageao, J.-F. Blavier, Y. Jiang, V. Nemtchinov, and S. P. Sander are with the Jet Propulsion Laboratory, California Institute of Technology, Pasadena, California 91109

S. P. Sander is also associated with the Division of Geological and Planetary Sciences and the Division of Engineering and Applied Sciences, California Institute of Technology, Pasadena, CA 91125

J. P. McGuire is with the Optical Research Corporation, Pasadena, California 91107

Figure Captions:

Figure 1: FTUVS instrument system at the NASA/JPL Table Mountain Facility

Figure 2: FTUVS interferometer subsystem schematic

Figure 3: East – West limb Doppler differencing technique (figure from Iwagami et al.[13]) used in this work

Figure 4: Spectral retrieval of telluric OH solar lines using solar Doppler differencing

Upper row: Positions and relative intensities of strong OH lines,

Middle row: East solar limb spectrum (curve to left in each panel), West spectrum (centered curve) and shifted East spectrum (matched to centered curve),

Bottom row: Ratio spectra (with residuals) and fitted OH reference spectra (simple curve).

Figure 5: Diurnal OH column abundance versus airmass measured on August 11, 1999

Figure 6: Estimated FTUVS acquired 15-minute average OH column uncertainties

FTUVS INSTRUMENT INSTALLATION AT TABLE MOUNTAIN FACILITY

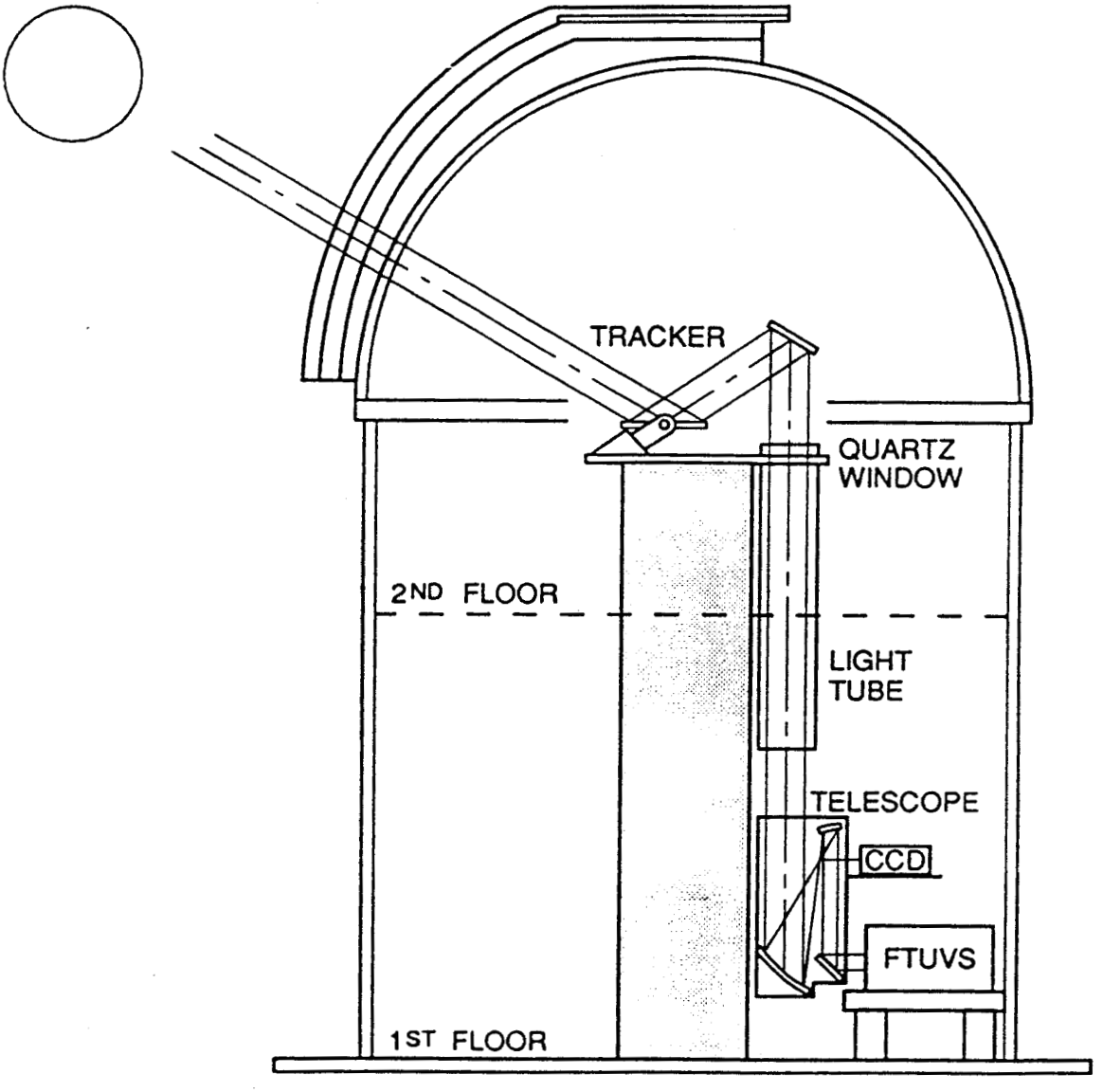

Figure 1

R. P. Cageao
Applied Optics

FOURIER TRANSFORM ULTRAVIOLET SPECTROMETER

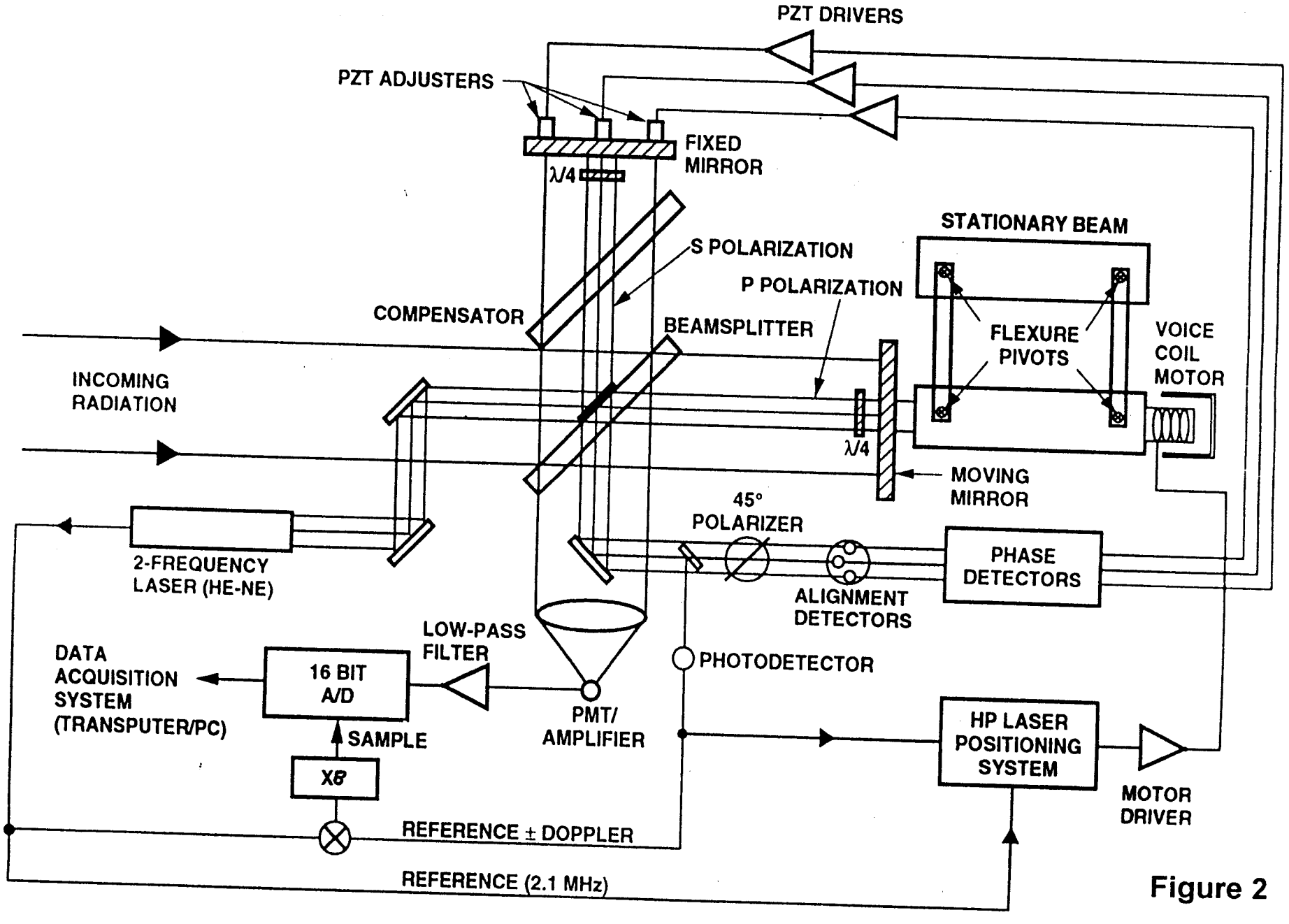

Figure 2

R. P. Cageao

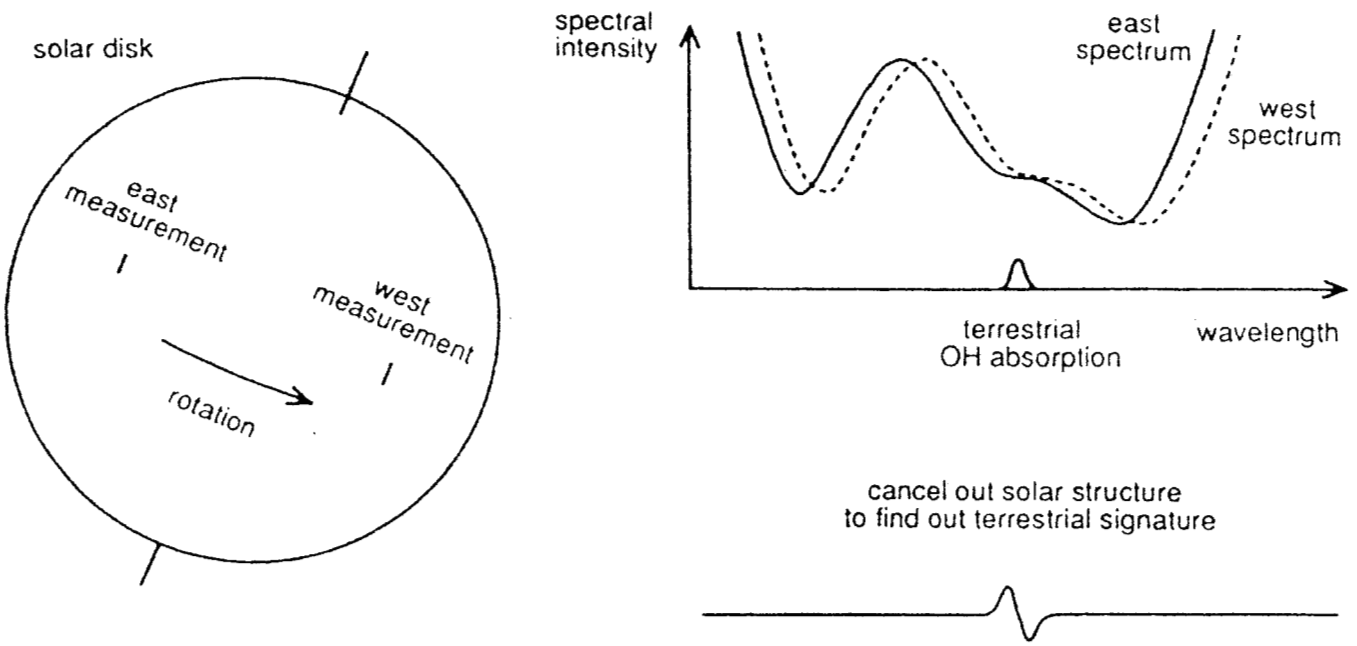

Figure 3

R. P. Cageao
Applied Optics

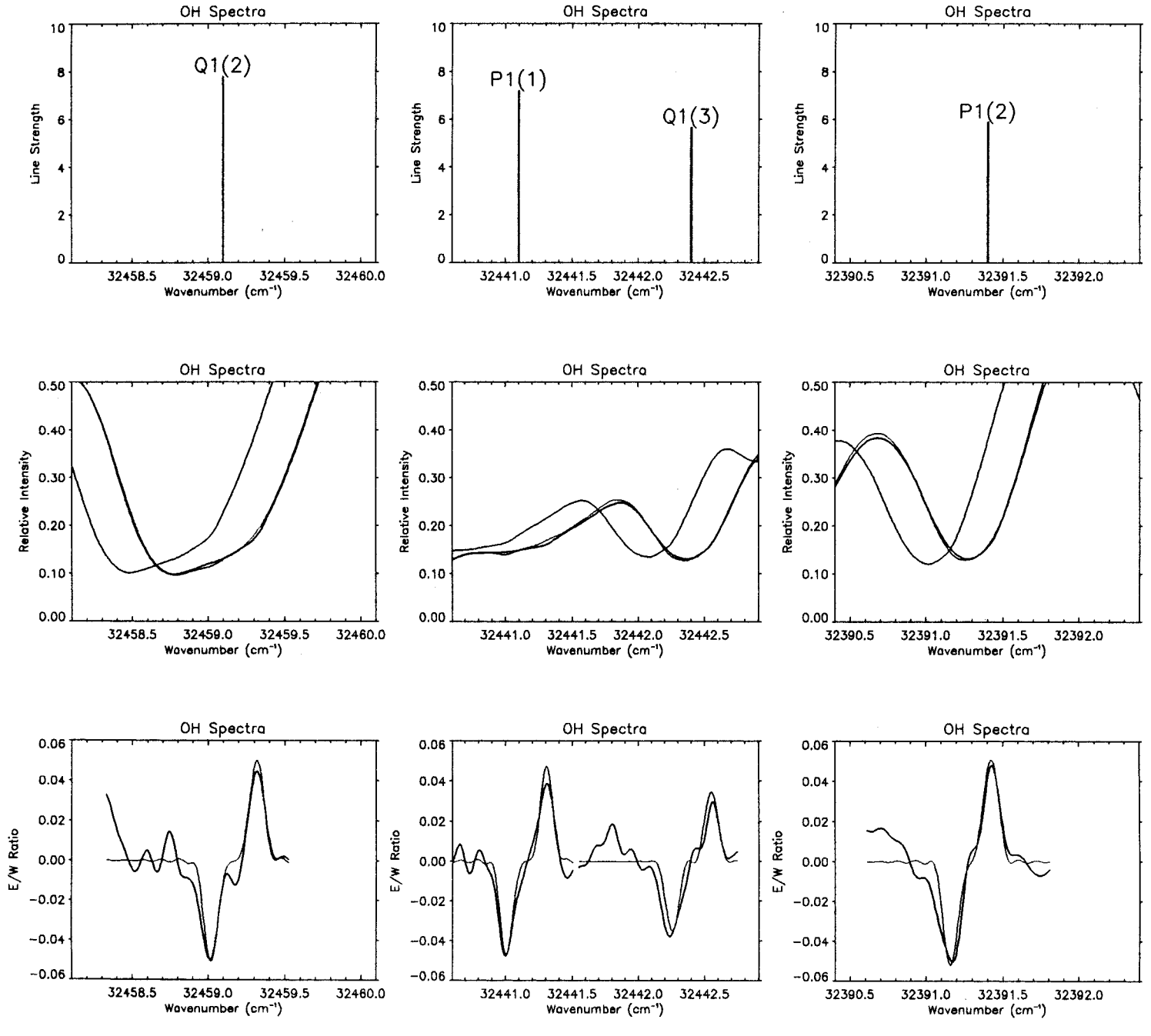

Figure 4

R. P. Cageao
Applied Optics

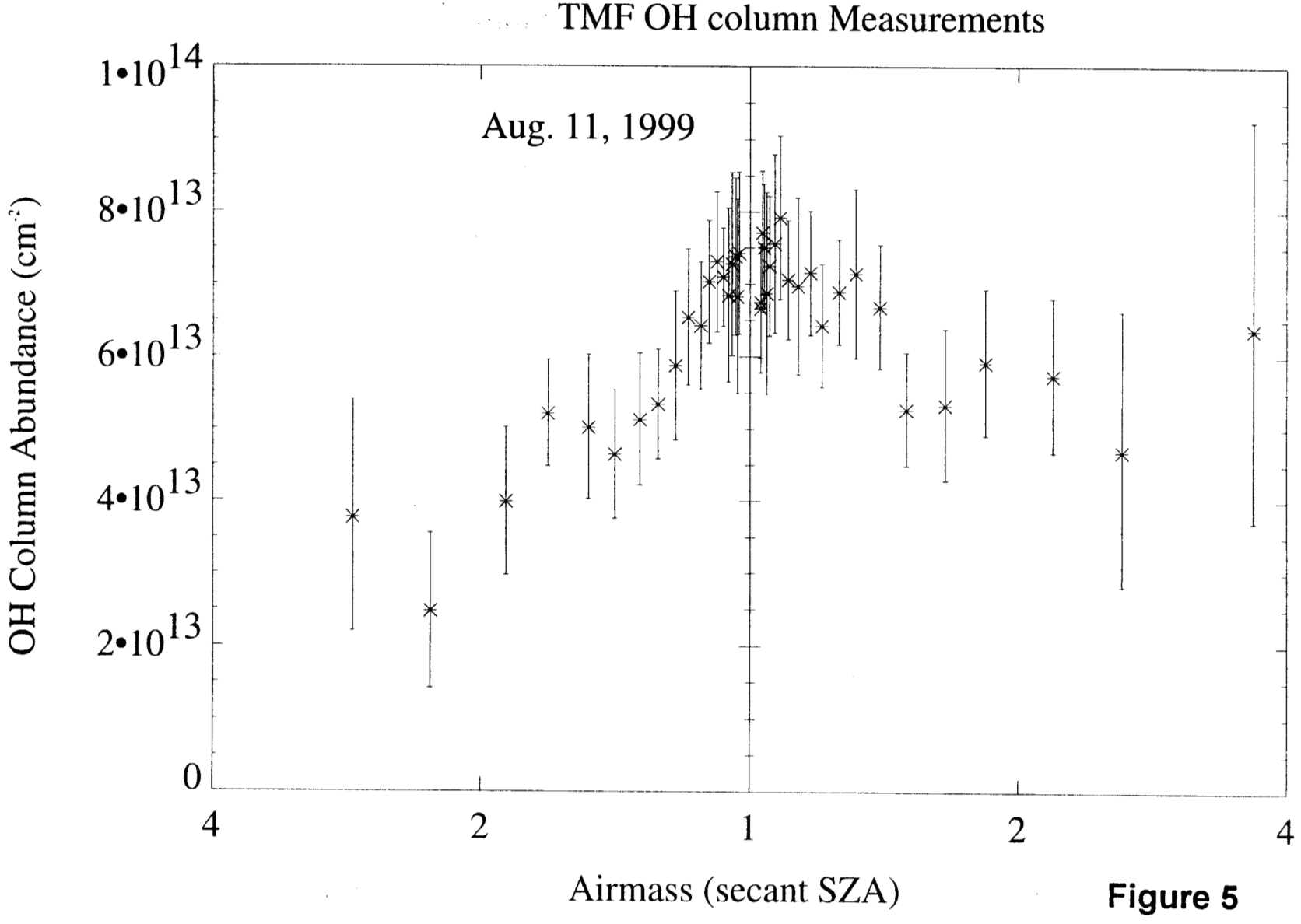

Figure 5

R. P. Cageao

FTUVS OH Column Measurement Uncertainty

ERROR Sources	Estimate	Description
Systematic		
Line Center Cross Section	±3 - 10%	OH vibrational level measured lifetime uncertainty (Dorn et al. 1995, Cageao et al. 1997).
	±7%	Stratospheric temperature uncertainty in column.
Constraining the fit (Least Squares χ^2 optimization)	±15%	Match observed spectra with modeled line shape. Residuals assessed using a χ^2 minimization with ± 5% error bars.
Other Absorptions	±?%	Possible unidentified absorption features at the location of OH lines.
Random		
Spectral Distortions	±5 - 10%	Instrument stability, air currents, acoustic and electronic noise.
Photon Noise	±2%	Poisson counting statistics.
Pointing System	±10%	Positioning drift on sun. Spectrum Doppler shift changes. Integrated solar spectrum shape affected.
TOTAL	±20 - 22%	

Figure 6

R. P. Cageao
Applied Optics

References:

1. P. O. Wennberg, R. C. Cohen, N. L. Hazen, L. B. Lapson, N. T. Allen, T. F. Hanisco, J. F. Oliver, N. W. Lanham, J. N. Demusz, and J. G. Anderson, "Aircraft-borne, laser-induced fluorescence instrument for the *in-situ* detection of hydroxyl and hydroperoxyl radicals," Rev. Sci. Instrum. **65**, 1858-1876 (1994).

2. R. M. Stimpfle, P. O. Wennberg, L. B. Lapson, and J. G. Anderson, "Simultaneous, *in situ* measurements of OH and HO_2 in the stratosphere," Geophys. Res. Lett. **17**, 1905-1908 (1990).

3. H. M. Pickett and D. B. Peterson, "Stratospheric OH measurements with a far-infrared limb sounding spectrometer," J. of Geophys. Res. **98**, 20507-20515 (1993).

4. H. M. Pickett and D. B. Peterson, "Comparison of measured stratospheric OH with prediction," J. of Geophys. Res. **101**, 16789-16796 (1996).

5. W. A. Traub, K. V. Chance, D. G. Johnson, and K. W. Jucks, "Stratospheric spectroscopy with the far-infrared spectrometer (FIRS-2)," Soc. Photo Opt. Instrum. Eng. **1491**, 298-307 (1991).

6. D. G. Johnson, K. W. Jucks, W. A. Traub, and K. V. Chance, "Smithsonian stratospheric far-infrared spectrometer and data reduction system," J. of Geophys. Res. **100**, 3091-3106 (1995).

7. R. R. Conway, D. K. Prinz, and G. H. Mount, "Middle Atmosphere high resolution spectrograph," SPIE **932**, 50-60 (1988).

8. R. R. Conway, M. H. Stevens, J. G. Cardon, S. E. Zasadil, C. M. Brown, J. S. Morrill, and G. H. Mount, "Satellite measurements of hydroxyl in the mesosphere," Geophys. Res. Lett. **23**, 2093-2096 (1996).

9. M. F. Morgan, D. G. Torr, and M. R. Torr, "Preliminary measurements of mesospheric OH $X^2\Pi$ by ISO on ATLAS I," Geophys. Res. Lett. **20**, 511-514 (1993).

10. C. R. Burnett and E. B. Burnett, "OH Pepsios," Appl. Opt. **22**, 2887-2892 (1983).

11. C. R. Burnett and E. B. Burnett, "Spectroscopic measurements of the vertical column abundance of hydroxyl (OH) in the Earth's stratosphere," J. Geophys. Res. **86**, 5185-5202 (1981).

12. C. R. Burnett and K. Minschwaner, "Continuing development in the regime of decreased atmospheric column OH at Fritz peak," Geophys. Res. Lett. **25**, 1313- (1998).

13. N. Iwagami, S. Inomata, I. Murata, and T. Ogawa, "Doppler detection of hydroxyl column abundance in the middle atmosphere," J. Atm. Chem. **20**, 1-15 (1995).

14. N. Iwagami, S. Inomata, and T. Ogawa, "Doppler detection of hydroxyl column Abundance in the middle atmosphere: 2. Measurement for three years and comparison with a 1D model," J. Atm. Chem. **29**, 195-216 (1998).

15. J. Notholt, H. Schutt, and A. Keens, "Solar absorption measurements of stratospheric OH in the UV with a Fourier-transform spectrometer," Appl. Opt. **36**, 6076-6082 (1997).

16. C. B. Farmer, "High resolution infrared spectroscopy of the Sun and the Earth's atmosphere from space," Mikrochim. Acta (Wien), **III**, 189-214 (1987).

17. G. C. Toon, "The JPL MkIV interferometer," Opt. Photon. News **2**, 19-21 (1991).

18. S. P. Sander, R. P. Cageao, and R. R. Friedl, "A compact, high resolution Michelson interferometer for atmospheric spectroscopy in the near ultraviolet," SPIE **1715**, 15-17 (1992).

19. R. P. Walker and J. D. Rex, "Interferometer design and data handling in a high-vibration environment. Part 1: interferometer design," SPIE **191**, 88-91 (1979).

20. C. R. Boucher and D. A. Naylor, "High resolution Fourier transform spectroscopy with phase correction in real time," Infra. Phys. **21**, 261-270 (1981).

21. M. L. Forman, W. H. Steel, and G. A. Vanasse, "Correction of asymmetric interferograms obtained in Fourier spectroscopy," J. Opt. Soc. Am. **56**, 59-63 (1966).